Multichannel Symbolic Aggregate Approximation Intelligent Icons: Application for Activity Recognition

Lamprini Pappa
Department of Informatics and Telecommunications, University of Ioannina
Arta, Greece
pappa.l@kic.uoi.gr

Petros Karvelis
Department of Informatics and Telecommunications, University of Ioannina
Arta, Greece
pkarvelis@uoi.gr

George Georgoulas
Department of Informatics and Telecommunications, University of Ioannina
Arta, Greece
georgoul@gmail.com

Chrysostomos Stylios
Department of Informatics and Telecommunications, University of Ioannina
Arta, Greece
stylios@uoi.gr

***Abstract*—In this work, we introduce the Multichannel Intelligent Icons, a novel method for producing and presenting essential patterns of multidimensional bio-signals. The proposed approach is an extension of Symbolic Aggregate Approximation (SAX) along with an innovative variation of Intelligent Icons. The innovation on the approach stands on the grounds of creating a spatial correlation of the inherited information in all dimensions and so it provides extra features for distinguishing the human activities. The proposed model is testing on Human Activity recorded data and for the classification purposes a Nearest Neighbour classifier is applied. The achieved results are compared with the case of applying single-channel intelligent icons approach and it is inferred a noteworthy increase in terms of accuracy and sensitivity with the proposed approach.**

Keywords—Human Activity Recognition, Symbolic Aggregate Approximation, Multichannel Intelligent Icons, Classification.

I. INTRODUCTION

In recent years there has been a great deal of interest in analyzing and monitoring peoples' daily activities so that to better understand their health conditions, provide help in times of need and/or prevent serious health problems [1]. Promoting healthier lifestyles (e.g. encouraging exercising), preventing stressful activities, detecting anomalous human behaviors (e.g. fall detection) or tracking health conditions (e.g. mobility worsening due to ageing or illnesses) are some of the various cases that profit from monitoring and inference of human health behavior [1]. Everyday human activity behavior modeling is implemented through a process called Human Activity Recognition (HAR) [2]. HAR is defined as the automatic detection of any everyday physical activities. The daily activities such as walking, running, sitting, lifting, climbing stairs up and down, cycling, etc. are easily identified using sensors that gather the various signals describing any human movement [1].

Researchers divide activities into static, dynamic, and transitional. Static activities are those whose the posture is stable for a period of time such as standing. Dynamic activities include physical movement such as walking. Transitional activities are restricted to changing between static activities, e.g. the transition between standing and sitting [3].

HAR is mainly distinguished in two types: video-based HAR and sensor-based HAR. The first one analyzes videos containing human motions captured with camera [4], whereas sensor-based HAR take advantage of sensors such as an accelerometer, gyroscope, sound sensors, etc. Due to the rapid growth of sensor technology, sensor-based HAR is constantly gaining ground [5].

One of the main directions to design and develop models capable of recognizing human activity is the usage of machine learning methods. Machine learning methods seem to offer better results in the extraction of information and in the recognition of an activity compared to the techniques derived from mathematics and statistics [6]. The solutions proposed based on machine learning algorithms range from the shallow algorithms to the deep learning algorithms lately [7].

Shallow algorithms manually configure the data segmentation, the noise reduction, the feature extraction and feature selection steps, while deep learning algorithms are able to implement all the above mentioned automatically. This resulted in the increase of the efficiency of classification models and the reduction of the human influence on HAR solutions. The main issue for both is the need of high computational resources related to memory and processing, especially for applying deep neural networks [5, 7].

The attempts to represent time series as symbols arose from the fact that the conversion of real signals into discrete ones gives to the researchers the opportunity to make use of the vast wealth of algorithms that have been implemented to handle similar representations [8]. Furthermore, symbolic representation algorithms allow a massive amount of data to be reduced down to a reasonable and representative number of symbols [9]. This contributes in the reduction of the complexity and computational cost of HAR solutions.

Symbolic Aggregate Approximation (SAX) method is an approach that allows the transformation of time series into symbols [9]. With this technique, the dimensionality of the problem is reduced, which positively affects the speed and efficiency of the machine learning algorithms used [10]. In addition, distance measures (in the symbolic space) can be used in correspondence to the distance measures of the original time series [9]. Finally, with the applied method for calculating the Euclidean distance there is a lower bounding guarantee [11]. A further step of SAX that has been introduced is intelligent icons technique for allowing lite-weight visualization and data mining [12].

Some applications of SAX that we came across during the literature review, include the diagnosis of rolling element bearings [13] and the automated detection of phasic activity

978-1-7281-2547-3/20/$31.00

during sleep [14], while another one takes into account the measurement uncertainty of the method [15].

In this work we introduce a novel method for constructing the intelligent icons in the case of multi-dimensional signals. While the single-channel method [12] builds one matrix for each dimension, the proposed approach simultaneously takes into account all the dimensions and creates the relevant matrix. Thus, the signal is described more effectively as the information is derived from all dimensions. We will demonstrate that our method presents better results in a HAR classification problem in comparison to the single-channel SAX approach.

The rest of this paper is organized as follows. Section II presents the basic steps of the method we propose. Section III describes the nature of the tested signals and the necessary processing we applied. In section IV we describe the Piecewise Aggregate Approximation, while in section V the SAX discretization stage takes place. Section VI provides the basic idea of computing intelligent icons and in section VII we present the proposed integrated method for symbolic representation. Section VIII is dedicated to describe the classification method we apply and section IX provides a brief description of the database we used and the data containing. In section X we demonstrate the evaluation of the method using some classification metrics. Section XI concludes the paper with directions for future work.

II. METHODS

The proposed method consists of the following steps. First, we preprocess the raw signals (accelerometer, gyroscope) by applying noise removal filters for signal smoothing. Right after that, the signals are being standardized and data segmentation is following that leads to an ensemble of windows. Then the Piecewise Aggregate Approximation (PAA) procedure is employed in order to reduce the dimension of the signal. PAA is an intermediate step that leads to the core of the Symbolic Aggregate Approximation (SAX) method, i.e. the discretization phase, where a string of symbols is produced for each window of the signal. The last step is the computation of the intelligent icons, where we compute them using both the single-channel SAX technique and the here proposed method. The latter are combined to form a table of features that consist the input of a KNN classifier that predicts the class (activity) of inputs. Fig. 1 illustrates the main steps of the integrated method.

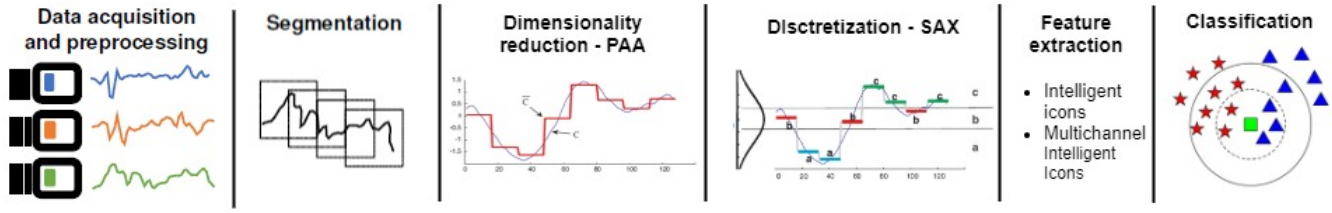

Fig. 1. The overall structural processing steps for the proposed method

III. SIGNAL USED

The proposed method is tested with signals from a publicly available web database [16, 17] that contains triaxial linear acceleration and angular velocity signals recorded from the accelerometer and the gyroscope of the device at a sampling rate of 50 Hz. This rate is sufficient for capturing human body motion since 99% of its energy is contained below 15Hz [18]. These signals were recorded by fifteen subjects conducting eight different activities: climbing stairs down and up, jumping, lying, standing, sitting, running/jogging, and walking. The signals were recorded in three axes. Fig. 2 illustrates a fraction of accelerometer and gyroscope signals for x, y, z axes respectively, from a randomly chosen activity (running).

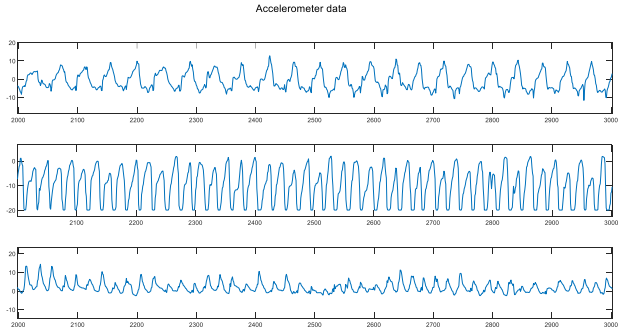

(a)

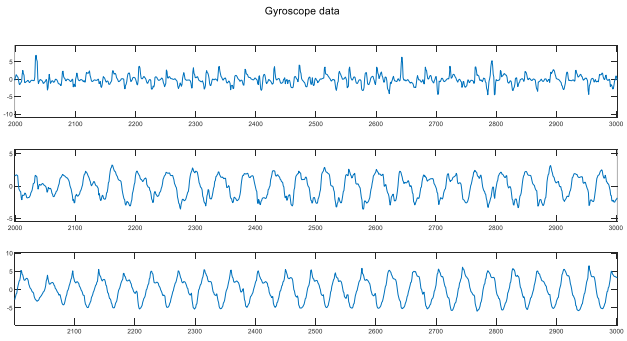

(b)

Fig. 2 Accelerometer signal (a) and gyroscope signal (b) (1000 points depiction), x, y, z directions respectively for the running activity

A. Pre-processing

The first step in the preprocessing phase is the synchronization of sensor data. This is necessary when multiple sensors are used, since the data from the sensors are not all received at the same time. The procedure that is described below is followed for each of the three discrete signals of each sensor, so we handle six separate signals. Fig. 3 illustrates the accelerometer signal for the x-dimension derived from the first subject of the database recorded when running.

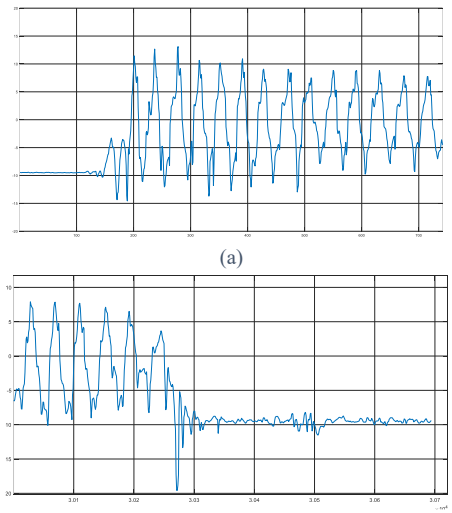

Fig. 3. Illustration of the beginning (a) and the end (b) of the accelerometer signal.

One can easily observe at Fig. 3, that at the beginning and at the end of the accelerometer signals there is a small part that did not resemble the pattern of the rest of the signal, but it shows relative calmness. This is a transitional condition that it normally occurs until each person enters the normal pace of the activity. Since these parts do not contain information that describe any activity, we exclude them. More specifically, 2% of all points are deducted from the beginning and the end of the signals. The latter percentage resulted after conducting tests with the objective the less possible useful signal be lost. The same procedure is followed for the gyroscope signals.

Afterwards, raw data are filtered using a fifth order median filter [19] and a fifth order low-pass Butterworth filter with a 20 Hz cutoff frequency [2, 20]. Fig. 4 displays the signal before and after applying the previously mentioned filters.

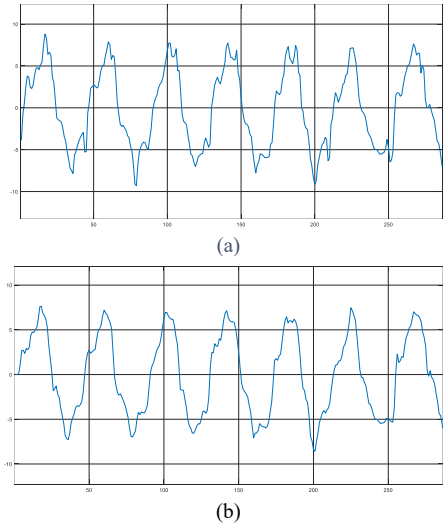

Fig. 4. The filtering process (a) The original and (b) the noise canceled accelerometer signal respectively

B. *Standardisation*

After the filtering of the signal, i.e. accelerometer, gyroscope, a z-score normalization step takes place. This is a standard procedure for the SAX algorithm in order to remove the distortions, namely the offset translation and the amplitude scaling, that has negative impact on the results of the activity recognition tasks [21].

We z-normalize each time series to have a mean of zero and a standard deviation of one since it is meaningless to compare time series with different offsets and amplitudes [11]. Eq. (1) is used to z-normalize the time series [22].

$$T_{norm} = \frac{T - \mu}{\sigma} \quad (1)$$

where: T is the original time series, μ is the mean value of time series variables, and σ is the standard deviation of the time series variable.

C. *Data segmentation*

We segment the filtered and standardized signal into sliding windows of the same size [23, 24]. The time windows are segmented successively without overlapping and with overlapping of 50% degree, in order to compare both cases for our test data. On the one hand, the overlapping technique provides us more data for training our classification model, and on the other hand the time series are scanned thoroughly, thus avoiding the loss of critical points that characterize the signal.

We choose the time window duration to be 2.56 seconds. Taking into account that the sampling frequency of the signal is 50 Hz, we can easily calculate the number of data points that consist a window, that is 50 Hz * 2.56 sec = 128 data points. Fig. 5 illustrates the segmentation into windows of 128 data points.

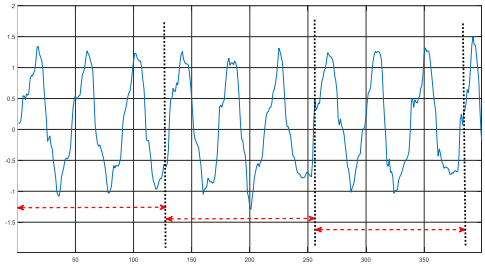

Fig. 5. Window Segmentation for the signal

Then, by considering that the filtered signal is an L-length time series and N is the number of points that we have chosen to make up a window, therefore the number of windows W that the time series is divided is given by $W = \frac{L}{N}$.

IV. Piecewise Aggregate Approximation

Below, for consistency, we list the symbols we use in our analysis.

L: Length of the time series
N: Window length
W: Number of windows the time series is segmented
n: Number of symbols of each window
α : Size of alphabet

Right after the segmentation, the PAA algorithm [8, 11] is applied to reduce the data dimensionality. The PAA steps are described below:

1. Choose the number of symbols n that represent each window.
2. Divide each window into n segments of length N/n.
3. Calculate the mean value of data points in every segment, given by Eq. (2)

$$\bar{x}_i = \frac{n}{N}\sum_{j=\frac{N}{n}(i-1)+1}^{\frac{N}{n}i} x_j \qquad (2)$$

where: $\bar{x}_i$ is the mean value of every segment, x_j is the given value of data point j, N is the number of data points in a window, and n is the number of symbols represent the window.

As a consequence, from each window a vector of length n is derived. These are the PAA coefficients.

In this specific analysis, we have chosen $n = 32$, so each window is represented by 32 symbols. As a result, the compression ratio is 128 / 32 = 4. Fig. 6 depicts the signal and its PAA illustration for a specific window.

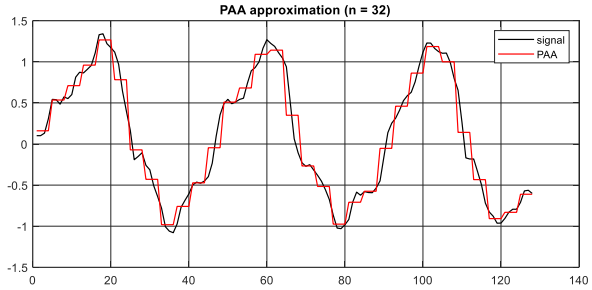

Fig. 6. Signal and PAA depiction (single window)

V. SAX - Discretization Stage

During the discretization stage, we essentially assign a symbol to each PAA coefficient, which has produced at the previous step. To do this, we select the size of the alphabet α. In other words, if we choose the number of symbols e.g. $\alpha = 4$, then each PAA coefficient can be represented by one of the following symbols 'a', 'b', 'c', 'd'.

Each symbol must have an equal probability of occurrence [8]. This condition is ensured by the fact that the samples after normalization follow the same normal distribution. Based on the size of the alphabet size we can choose the cut zones β_i (breakpoints) obtained from the table of normal distribution [25] as shown at Fig.7. Breakpoints define a bin in which an alphabet letter is assigned.

In the PAA stage, we set the n = 32 for each window. We match each value to a symbol based on the region it belongs. In this way a window is now represented by a sequence of symbols, in other words we transformed our problem from a real value problem to string problem. Fig. 8 comprehensively illustrates the procedure described and its results.

β_i \ a	3	4	5	6	7	8	9	10
β_1	-0.43	-0.67	-0.84	-0.97	-1.07	-1.15	-1.22	-1.28
β_2	0.43	0	-0.25	-0.43	-0.57	-0.67	-0.76	-0.84
β_3		0.67	0.25	0	-0.18	-0.32	-0.43	-0.52
β_4			0.84	0.43	0.18	0	-0.14	-0.25
β_5				0.97	0.57	0.32	0.14	0
β_6					1.07	0.67	0.43	0.25
β_7						1.15	0.76	0.52
β_8							1.22	0.84
β_9								1.28

Fig. 7. Lookup table that contains the breakpoints

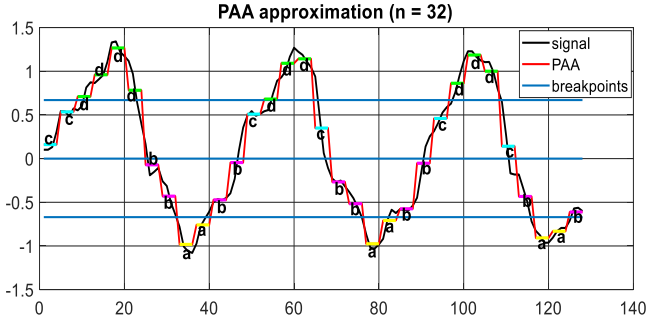

Fig. 8. Signal, PAA, breakpoint lines, symbols illustrated all together

Finally, the string produced after applying SAX is provided below (referring to a single window).

S = 'ccddddbbaabbcdddcbbaabbcdddcbaab'

and in a colorized format S =

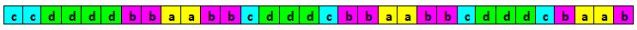

VI. Intelligent Icons

Intelligent icons are a method that visualize the results after applying SAX [12]. In this way, we compute the frequency of occurrence of a symbol or group of symbols (called words) within a window creating approximations of the underlying probability mass functions [26]. The steps are described below:

- Define the word length, that is the number of symbols that can form a word. In our analysis we have chosen after testing (considering the efficiency and complexity of the method and finding the middle ground) the word length = $l = 3$.
- Compute all possible combinations of alphabet symbols that define the possible words. In our experiment, since $l = 3$ and $\alpha = 4$, the total number of combinations is 64.
- For each word, we compute the number of occurrences in the string generated after the implementation of SAX for every window separately.
- Create a 2-dimension histogram matrix that describes the frequency of each word, as shown at Fig. 9.

Fig. 9 shows a visual representation of an intelligent icon.

aaa	aca	baa	bca	caa	cca	daa	dca
aab	acb	bab	bcb	cab	ccb	dab	dcb
aac	acc	bac	bcc	cac	ccc	dac	dcc
aad	acd	bad	bcd	cad	ccd	dad	dcd
aba	ada	bba	bda	cba	cda	dba	dda
abb	adb	bbb	bdb	cbb	cdb	dbb	ddb
abc	adc	bbc	bdc	cbc	cdc	dbc	ddc
abd	add	bbd	bdd	cbd	cdd	dbd	ddd

(a)

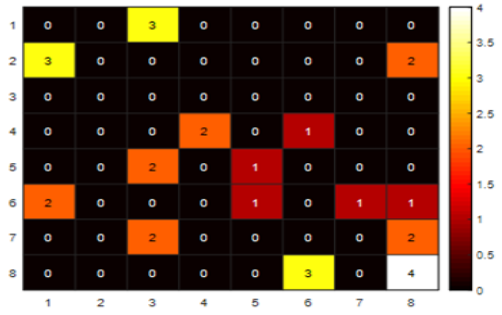

(b)

Fig. 9. (a) The table of all combinations and (b) the single-channel intelligent icon (with correspondence to the above table) derived from the string S = 'ccd dddbbaabbcdddcbbaabbcdddcbaab'. Each number shows the frequency of occurrence of the triplet that is in the corresponding cell.

VII. Multichannel Intelligent Icons

Here, we introduce the multichannel Intelligent Icons modeling approach, which is an extension and innovative approach to the single-channel intelligent icon representation [12]. The novelty comes when producing the intelligent icons which are now formed by finding all possible words that come from combining symbols through all dimensions, that is, x, y, z. In other words, we construct the correlated intelligent icons along with the three directions of the signal. In the following we describe the proposed procedure in more detail:

Let us focus on the first window of x, y and z dimension of the accelerometer signal obtained from the first subject of the database while running. After applying SAX, we extract three different strings for each one of the different dimensions.

x axis: 'ccddddbbaabbcdddcbbaabbcdddcbaab'

y axis: 'aaccdaabdddaacccabcddbabddbacddc'

z axis: 'cbaaabcbbabdbbaabcbbbcdcbabbbabc'

We now search for words (made of 3 symbols) where the first symbol comes from x-string, the second from y-string and the third from z-string, as shown in Fig. 10.

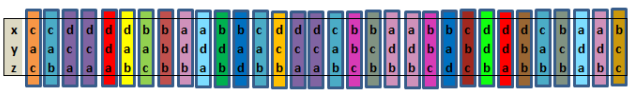

Fig. 10. Words are consisted of one symbol from every dimension for computing multichannel intelligent icon

The frequency of occurrence of all the words, while reading words with the above-mentioned way, constitutes the multichannel intelligent icon. Fig. 11 depicts the generated multichannel intelligent icon.

aaa	aca	baa	bca	caa	cca	daa	dca
aab	acb	bab	bcb	cab	ccb	dab	dcb
aac	acc	bac	bcc	cac	ccc	dac	dcc
aad	acd	bad	bcd	cad	ccd	dad	dcd
aba	ada	bba	bda	cba	cda	dba	dda
abb	adb	bbb	bdb	cbb	cdb	dbb	ddb
abc	adc	bbc	bdc	cbc	cdc	dbc	ddc
abd	add	bbd	bdd	cbd	cdd	dbd	ddd

(a)

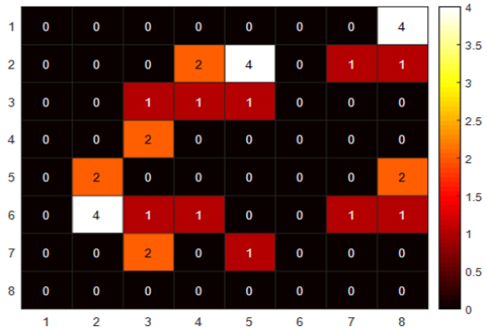

(b)

Fig. 11. (a) The table of all combinations and (b) the multichannel intelligent icon (with correspondence to the above table). Each number shows the frequency of occurrence of the triplet that is in the corresponding cell.

We are proposing the following algorithm in order to produce the Multichannel Intelligent Icons. The proposed steps are:

Step 1: Apply SAX on each dimension of a *p*-dimensional signal (separately).
Step 2: Obtain *p* unique strings.
Step 3: Transversal search for words of length *p* through all strings.
Step 4: Compute the Intelligent Icons table that contains α^p elements.

VIII. Classification

After deriving the intelligent icons (single-channel and multichannel ones) from every window and every dimension of the signals used, we have to build the table of features that will be the input of the classifier [27]. For this purpose, we place the tables of single-channel intelligent icons and multichannel intelligent icons horizontally side by side with the following sequence:

- accelerometer signal - single-channel intelligent icon approach
  - - x dimension
  - - y dimension
  - - z dimension
- gyroscope signal - single-channel intelligent icon approach
  - - x dimension
  - - y dimension
  - - z dimension

- accelerometer signal - multichannel intelligent icon approach
- gyroscope signal - multichannel intelligent icon approach

We employed a Nearest Neighbour classifier consisting of one neighbour in order to examine the prediction accuracy of the model. We randomly separated the table of features to obtain a training dataset and a testing dataset. The training dataset consists of randomly extracted 80% of the intelligent icons of every class and the remaining 20% constitutes the testing dataset.

IX. DATA SET USED

The database [16,17] contains signals that were recorded by fifteen subjects who performed eight different activities: climbing stairs down and up, jumping, lying, standing, sitting, running/jogging, and walking. Here, we only used the signals produced from the accelerometer and the gyroscope of the device. The sampling rate was set at 50 Hz. The data set covers acceleration and gyroscope data of the activities climbing stairs down and up, jumping, lying, standing, sitting, running/jogging, and walking of fifteen subjects (age 31.9±12.4, height 173.1±6.9, weight 74.1±13.8, eight males and seven females). Each subject performed each activity roughly for 10 minutes except from jumping due to the physical exertion (~1.7 minutes). Concerning the gender, the amount of data is equally distributed [16, 17]. The file of the activity "Climbing stairs up" is empty for the second subject. We just ignored this one.

X. RESULTS

We repeated the execution of the Nearest Neighbour algorithm ten times and Table I depicts the overall classification accuracy of the proposed model and the relevant standard deviation (STD).

TABLE I. Accuracy of the proposed model for no-overlapping and overlapping sliding windows approach for the proposed method

ACCURACY (%)			
no – overlapping windows		***50% overlapping windows***	
MEAN	*STD*	*MEAN*	*STD*
84.42	0.42	92.39	0.24

Fig. 12 illustrates the confusion matrices and the average TPR for every activity.

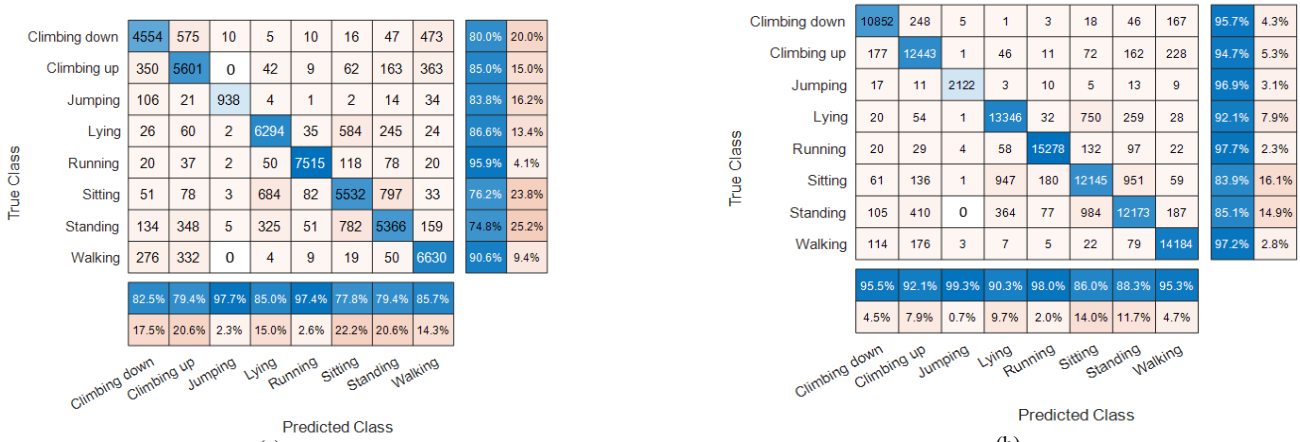

Fig. 12. Total confusion matrices of (a) no-overlapping sliding windows approach and (b) 50% overlapping sliding windows approach of the proposed method. The last two columns display the percentage of correctly and incorrectly classified observations for each predicted class. The last two rows display the percentage of correctly and incorrectly classified observations for each true class.

For comparison purposes, we carried out the single-channel intelligent icon computation approach with exact the same dataset, the exact same classifier and the same number of repetitions for testing the latter. In short, the results are presented in Table II and Fig. 13.

TABLE II. Accuracy of the single-channel model for no-overlapping and overlapping sliding windows approach for single-channel computation of intelligent icons

ACCURACY (%)			
no – overlapping windows		***50% overlapping windows***	
MEAN	*STD*	*MEAN*	*STD*
81.10	0.39	90.13	0.20

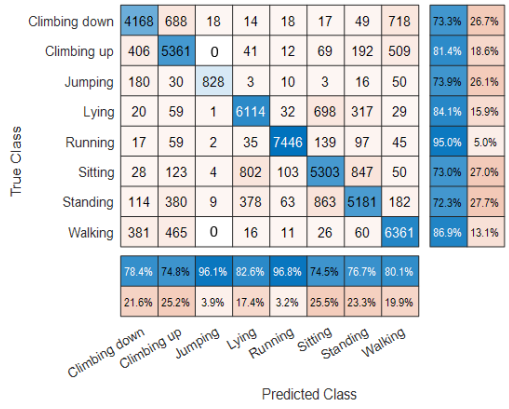

(a)

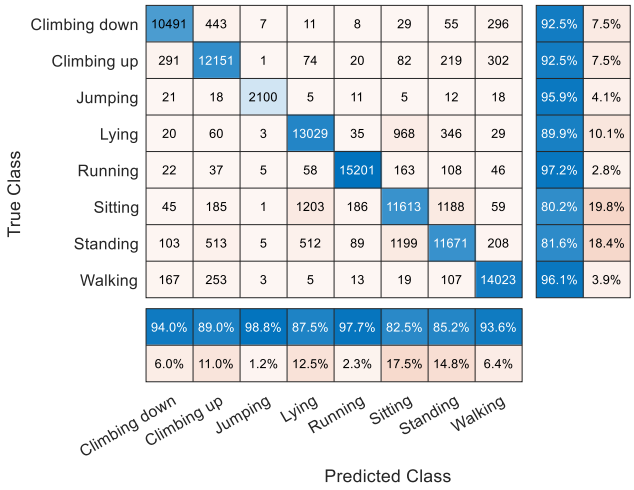

(b)

Fig. 13. Total confusion matrix of (a) no-overlapping sliding windows approach and (b) 50% overlapping sliding windows approach for single-channel method. The last two columns display the percentage of correctly and incorrectly classified observations for each predicted class. The last two rows display the percentage of correctly and incorrectly classified observations for each true class.

Table III depicts the comparative average and standard deviation values [28] of TPR between the two approaches, our method and single-channel intelligent icons, for no-overlapping and overlapping sliding windows experiments. At a first glance at Table III, we can observe that our method achieved an increase on both overall accuracy and sensitivity in both overlapping and no-overlapping sliding windows approaches at a level of 3%. The activities presenting the most increase in accuracy are "climbing up", "sitting" and "standing". These are easily confused, the first one with "climbing down" and the two left together. It is shown in confusion matrices in Fig. 12, 13 that there exists a leakage between these easily confused activities. This is a common problem as it is justified in other works, that is distinguishing the "sitting" and "standing" activities which are often described as non-dynamic activities [2] and the "climbing down" and "climbing up" activities [29]. However, as shown in Fig. 12, 13 multichannel signals can actually better describe the relative stillness of non-dynamic activities correlated in space reducing the possible leakages to other closely related activities (false positives). In general, the feature table derived from our method acts as a distinguishing factor between similar activities.

The overlapping-windows approach has evidently better performance than the no-overlapping windows one. Let us comment on the increase of "climbing down" (~15.7%) and "standing" (~11%). In connection to what mentioned in the previous paragraph, the overlap clearly provides the datapoints that are crucial for distinguishing these easily misclassified activities. Another noteworthy increase (~13%) occurs at activity "jumping" where we observe a false positive leakage to "climbing down" mainly. This could be explained if we take into consideration that this activity consists of the fewer samples, consequently it is vulnerable to be overridden by other activities in the nearest neighbour classification step. Thus, overlapping-windows boosts the prediction ability of this activity and restricts the above explained leakage. Another finding is that the two activities that outperform is running and walking exceeding 97% TPR. They are dynamic activities and consequently the easiest to predict as they present distinct attributes. Moreover, our method presents lower standard deviation values in general, meaning that its results are more concentrated, more robust, thus more reliable.

TABLE III. Total comparative table between our method and single-channel intelligent icons approach

ACTIVITIES	Our Method				Single-channel Intelligent Icons Approach			
	TPR (%)		*STD (%)*		*TPR (%)*		*STD (%)*	
	No-overlap	*Overlap*	*No-overlap*	*Overlap*	*No-overlap*	*Overlap*	*No-overlap*	*Overlap*
Climbing down	80.04	95.70	1.27	0.63	73.25	92.51	1.24	0.88
Climbing up	84.99	94.70	1.20	0.98	81.35	92.47	1.47	1.04
Jumping	83.75	96.89	2.79	0.91	73.93	95.89	2.18	1.18
Lying	86.57	92.10	1.19	0.37	84.10	89.92	1.29	0.74
Running	95.85	97.69	0.63	0.46	94.97	97.19	0.68	0.44
Sitting	76.20	83.87	1.11	0.59	73.04	80.20	1.49	0.75
Standing	74.84	85.13	1.44	0.91	72.26	81.62	0.97	1.03
Walking	90.57	97.22	1.48	0.33	86.90	96.11	1.39	0.50
MEAN	**84.10**	**92.91**	**1.39**	**0.65**	**79.98**	**90.74**	**1.34**	**0.82**

XI. CONCLUSIONS

This study introduces the hybrid Intelligent Icons technique which is successfully applied for Human Activity Recognition. A new feature table of multichannel intelligent icons is generated after applying the proposed method and it is integrated to the table of single-channel intelligent icons. All features are inputs to a classifier. The results of our experiments, obtained after performing Nearest Neighbour classification, indicate that the proposed approach achieves improved accuracy and sensitivity rates compared to the approach using just only single-channel intelligent icons. It is also mentioned that the difficulty in distinguishing relative activities is overcome. The proposed method excels in predicting and recognizing dynamic human activities. Moreover, it is concluded that applying overlapping sliding windows, it enhances the experimental outcomes for both single-channel and the proposed multichannel method.

In both the single-channel and the Multichannel Intelligent Icons approach, we must define the main parameters of the

algorithm i.e. alphabet size, word length. Here, we use a trial and error process for adjusting the values of parameters so that to choose the optimal values for conducting experiments.

In future work, we will investigate the proposed approach for imbalanced datasets. We will also investigate other human activity recognition tasks that are complex and are characterized with transitional activities showing relative difficulty in distinguishing them.

To conclude, we have proposed a semi-automated method (no feature selection is required) for recognizing human activities exhibiting high performance in terms of prediction accuracy utilizing data from just two sensors. The proposed and implemented algorithm is quite simple but it is intuitive, and it correlates movement in space. The simplicity offers relatively low computational and complexity costs making it a viable solution for using streaming data.

ACKNOWLEDGMENT

This research work is funded by the Operational Programme "Epirus" 2014-2020, under the project "Integrated Support System for elderly people with health problems and lonely workers using Portable Devices and Machine learning Algorithms – TrackMyHealth", Co-financed by the European Regional Development Fund (ERDF).

REFERENCES

[1] Banos, O., Galvez, J.-M., Damas, M., Pomares, H., & Rojas, I. (2014). Window Size Impact in Human Activity Recognition. Sensors, 14(4), 6474–6499. https://doi.org/10.3390/s140406474

[2] Anguita, D., Ghio, A., Oneto, L., Parra, X., & Reyes-Ortiz, J.L. (2013). A Public Domain Dataset for Human Activity Recognition using Smartphones. ESANN.

[3] Gao, L., Bourke, A. K., & Nelson, J. (2014). Evaluation of accelerometer based multi-sensor versus single-sensor activity recognition systems. Medical Engineering & Physics, 36(6), 779–785. https://doi.org/10.1016/j.medengphy.2014.02.012

[4] Cook, D., Feuz, K. D., & Krishnan, N. C. (2013b). Transfer learning for activity recognition: a survey. Knowledge and Information Systems, 36(3), 537–556. https://doi.org/10.1007/s10115-013-0665-3

[5] Wang, J., Chen, Y., Hao, S., Peng, X., & Hu, L. (2019). Deep learning for sensor-based activity recognition: A survey. Pattern Recognition Letters, 119, 3–11. https://doi.org/10.1016/j.patrec.2018.02.010

[6] Ramasamy Ramamurthy, S., & Roy, N. (2018). Recent trends in machine learning for human activity recognition-A survey. Wiley Interdisciplinary Reviews: Data Mining and Knowledge Discovery, 8(4), e1254. https://doi.org/10.1002/widm.1254

[7] Sousa Lima, W., de Souza Bragança, H., Montero Quispe, K., & Pereira Souto, E. (2018). Human Activity Recognition Based on Symbolic Representation Algorithms for Inertial Sensors. Sensors, 18(11), 4045. https://doi.org/10.3390/s18114045

[8] Lin, J., Keogh, E., Lonardi, S., & Chiu, B. (2003). A symbolic representation of time series, with implications for streaming algorithms. Proceedings of the 8th ACM SIGMOD Workshop on Research Issues in Data Mining and Knowledge Discovery - DMKD 03. doi: 10.1145/882082.882086

[9] Camerra, A., Palpanas, T., Shieh, J., & Keogh, E. (2010, December). iSAX 2.0: Indexing and mining one billion time series. In 2010 IEEE International Conference on Data Mining (pp. 58-67). IEEE.

[10] Schäfer, P., & Högqvist, M. (2012). Sfa. Proceedings of the 15th International Conference on Extending Database Technology - EDBT 12. doi: 10.1145/2247596.2247656

[11] Lin, J., Keogh, E., Wei, L., & Lonardi, S. (2007). Experiencing SAX: a novel symbolic representation of time series. Data Mining and Knowledge Discovery, 15(2), 107–144. https://doi.org/10.1007/s10618-007-0064-z

[12] Keogh, E., Wei, L., Xi, X., Lonardi, S., Shieh, J., & Sirowy, S. (2006). Intelligent Icons: Integrating Lite-Weight Data Mining and Visualization into GUI Operating Systems. Sixth International Conference on Data Mining (ICDM'06). https://doi.org/10.1109/icdm.2006.90

[13] Georgoulas, G., Karvelis, P., Loutas,T., Stylios, C., Rolling element bearings diagnostics using the Symbolic Aggregate approXimation. Mechanical Systems and Signal Processing, Volumes 60–61, August 2015, Pages 229-242, ISSN 0888-3270, DOI: 10.1016/j.ymssp.2015.01.033 (2015).

[14] Fairley, J., Karvelis, P., Georgoulas, G., Stylios, C., Rye D., and Bliwise, D., Symbolic Representation of Human Electromyograms for Automated Detection of Phasic Activity During Sleep. In: Proceedings of 2014 IEEE Statistical Signal Processing Workshop SSP'14, 29 June-2 July 2014, Gold Coast, Queensland, Australia (2014).

[15] Stylios C., and Kreinovich, V., Symbolic Aggregate ApproXimation (SAX) under Interval Uncertainty. In: Proceedings of 2015 Annual Conference of the North American Fuzzy Information Processing Society (NAFIPS) held jointly with 2015 5th World Conference on Soft Computing (WConSC), 17-19 Aug. 2015, Redmond, Washington, USA. DOI: 10.1109/NAFIPS-WConSC.2015.7284164 (2015).

[16] Sztyler, T., & Stuckenschmidt, H. (2016). On-body localization of wearable devices: An investigation of position-aware activity recognition. 2016 IEEE International Conference on Pervasive Computing and Communications (PerCom). doi: 10.1109/percom.2016.7456521

[17] Human Activity Recognition. (n.d.). Retrieved from https://sensor.informatik.uni-mannheim.de/#dataset_realworld

[18] Karantonis, D. M., Narayanan, M. R., Mathie, M., Lovell, N. H., & Celler, B. G. (2006). Implementation of a Real-Time Human Movement Classifier Using a Triaxial Accelerometer for Ambulatory Monitoring. IEEE Transactions on Information Technology in Biomedicine, 10(1), 156–167. https://doi.org/10.1109/titb.2005.856864

[19] Pitas, I., & Venetsanopoulos, A. N. (1990). Median Filters. Nonlinear Digital Filters, 63–116. https://doi.org/10.1007/978-1-4757-6017-0_4

[20] Bansal, M., Sharma, R., & Grover, P. (2010). Performance evaluation of Butterworth Filter for Signal Denoising. International Journal of Electronics & Communication Technology, December.

[21] Junejo, I. N., & Aghbari, Z. A. (2012). Using SAX representation for human action recognition. Journal of Visual Communication and Image Representation, 23(6), 853–861. https://doi.org/10.1016/j.jvcir.2012.05.001

[22] Bird, J. (2003). The normal distribution. In Engineering Mathematics (4th ed., pp. 340–346). Retrieved from https://doc.lagout.org/science/0_Computer%20Science/3_Theory/Mathematics/Engineering%20Mathematics%2C%204th%20ed.pdf

[23] Kozina, S., Lustrek, M., & Gams, M. (2011). Dynamic signal segmentation for activity recognition.

[24] Foster, J., Bevis, M., & Businger, S. (2005). GPS Meteorology: Sliding-Window Analysis. Journal of Atmospheric and Oceanic Technology, 22(6), 687–695. https://doi.org/10.1175/jtech1717.1

[25] Patel, P., Keogh, E., Lin, J., & Lonardi, S. (n.d.). Mining motifs in massive time series databases. 2002 IEEE International Conference on Data Mining, 2002. Proceedings. doi: 10.1109/icdm.2002.1183925

[26] Karvelis, P., Georgoulas, G., Tsoumas, I. P., Antonino-Daviu, J. A., Climente-Alarcon, V., & Stylios, C. D. (2015). A Symbolic Representation Approach for the Diagnosis of Broken Rotor Bars in Induction Motors. IEEE Transactions on Industrial Informatics, 11(5), 1028–1037. https://doi.org/10.1109/tii.2015.2463680

[27] Larose, D.T. and Larose, C.D. (2014). k-Nearest Neighbor Algorithm. In Discovering Knowledge in Data (eds D.T. Larose and C.D. Larose). doi:10.1002/9781118874059.ch7

[28] Gurland, J., & Tripathi, R. C. (1971). A Simple Approximation for Unbiased Estimation of the Standard Deviation. The American Statistician, 25(4), 30. https://doi.org/10.2307/2682923

[29] Artetxe, A., Beristain, A., & Kabongo, L. (2014). Activity Classification Using Mobile Phone based Motion Sensing and Distributed Computing. Studies in health technology and informatics, 207, 1-10